Oral presentation | Numerical methods

Numerical methods-I

Tue. Jul 16, 2024 2:00 PM - 4:00 PM Room A

[5-A-03] A node-conservative cell-centered Finite Volume method for solving multidimensional Euler equations over general unstructured grids

*Pierre-Henri Maire[1], Vincent Delmas[1,2], Raphaël Loubère[2] （1. CEA, 2. Institut de Mathématiques de Bordeaux ）

Keywords: Hypersonic flows, Finite Volume, Unstructured grids

A node-conservative cell-centered Finite Volume method for solving multidimensional Euler equations over general unstructured grids

ICCFD12 Kobe, July 14-19 2024

Pierre-Henri Maire (pierre-henri.maire@cea.fr)
DIRECTION DES APPLICATIONS MILITAIRES
CENTRE D'ETUDES SCIENTIFIQUES ET TECHNIQUES D'AQUITAINE, LE BARP FRANCE

Outline

Context and Motivations: Numerical Simulation of 3D Hypersonic Flows

The compressible Euler equations

Simple approximate Riemann solver

An unconventional cell-centered Finite Volume discretization

Multidimensional numerical results

Context and Motivations

Context

- **Numerical simulation of 3D hypersonic flows still a challenging task which requires a subtle balance between robustness and accuracy**
- On going work with Ph.D students: Agnes Chan [2019-2022] & Vincent Delmas [2023-2026]
- Co-supervisors: R. Loubère (CNRS/Institut de Mathématiques de Bordeaux) and PHM

Motivations

- Design **robust and accurate cell-centered Finite Volume (FV) methods** for solving multiD Euler & Navier-Stokes equations on **unstructured** grids
- Robustness cornerstone: Entropy stable and **positivity preserving approximate Riemann solvers** (RS) [G. Gallice, Numer. Math., 2002]
- Construction of multiD FV methods based on **node-centered approximate RS** extending the previous works devoted to
  - Lagrangian gas dynamics [R. Loubère, PHM, B. Rebourcet, HNMHP, 2016]
  - Eulerian gas dynamics [Z. Shen et al., J. Comp. Phys, 2014]

The compressible Euler equations

Governing equations

$$\frac{\partial \mathbf{U}}{\partial t} + \nabla \cdot \mathbb{F}(\mathbf{U}) = \mathbf{0},$$

$$\mathbf{U} = (\rho, \rho\mathbf{v}, \rho e)^t \in \mathbb{R}^{d+2},$$

$$\mathbb{F}(\mathbf{U}) = \begin{pmatrix} \rho\mathbf{v}^t \\ \rho\mathbf{v}\otimes\mathbf{v} + p\mathbb{I}_d \\ \rho e\mathbf{v}^t + p\mathbf{v}^t \end{pmatrix}.$$

Thermodynamic closure

- Specific internal energy $\varepsilon = e - \frac{1}{2}\mathbf{v}^2$
- Specific entropy η
- $(\tau,\eta) \longmapsto \varepsilon(\tau,\eta)$ strictly convex
- Complete equation of state

$$p(\tau,\eta) = -\frac{\partial\varepsilon}{\partial\tau}, \quad \theta(\tau,\eta) = \frac{\partial\varepsilon}{\partial\eta} > 0, \text{ temperature}$$

Main properties

- Hyperbolicity: $\frac{\partial \mathbb{F}(\mathbf{U})\mathbf{n}}{\partial \mathbf{U}}$ is diagonalizable for all unit vector $\mathbf{n}$ with the real eigenvalues

$$\Lambda_- = \mathbf{v}\cdot\mathbf{n} - a, \Lambda_0 = \mathbf{v}\cdot\mathbf{n}\,(\text{multiplicity d}), \Lambda_+ = \mathbf{v}\cdot\mathbf{n} + a, \text{ where } \frac{a^2}{\tau^2} = -\frac{\partial p}{\partial\tau}$$

- Entropy inequality

$$\frac{\partial\rho\eta}{\partial t} + \nabla\cdot(\rho\eta\mathbf{v}) \geq 0.$$

Riemann problem in the $\mathbf{n}$ direction ($\mathbf{n}^2 = 1$)

Riemann problem (RP)

$$\frac{\partial \mathbf{U}}{\partial t} + \frac{\partial \mathbf{F_n}}{\partial x_\mathbf{n}} = \mathbf{0}$$

$$\mathbf{U}(0, x_\mathbf{n}) = \begin{cases} \mathbf{U}_l \text{ if } x_\mathbf{n} < 0, \\ \mathbf{U}_r \text{ if } x_\mathbf{n} \geq 0, \end{cases}$$

where $\mathbf{F_n} = \mathbb{F}\mathbf{n}$ and $x_\mathbf{n} = \mathbf{x} \cdot \mathbf{n}$.

Entropy inequality

$$\frac{\partial \rho\eta}{\partial t} + \frac{\partial}{\partial x_\mathbf{n}}(\rho\eta\mathbf{v}) \geq 0.$$

Local notations

$$\mathbf{U} = \begin{pmatrix} \rho \\ \rho v_\mathbf{n} \\ \rho \mathbf{v}_t \\ \rho e \end{pmatrix} \text{ and } \mathbf{F_n} = \begin{pmatrix} \rho v_\mathbf{n} \\ \rho v_\mathbf{n}^2 + p \\ \rho v_\mathbf{n} \mathbf{v}_t \\ \rho v_\mathbf{n} e + p v_\mathbf{n} \end{pmatrix},$$

where $\mathbf{v} = v_\mathbf{n}\mathbf{n} + \mathbf{v}_t$.

Normal flux decomposition

$$\mathbf{F_n} = v_\mathbf{n}\mathbf{U} + \mathbf{L}(\mathbf{U}), \text{ where } \mathbf{L}(\mathbf{U}) = \begin{pmatrix} 0 \\ p \\ \mathbf{0} \\ p v_\mathbf{n} \end{pmatrix}$$

Simple approximate Riemann solver [Gallice, CRAS, 2002]

Simple Riemann solver

$$\mathbf{W}(\mathbf{U}_l, \mathbf{U}_r, \xi) = \begin{cases} \mathbf{U}_l \text{ if } \xi < \Lambda_l, \\ \mathbf{U}_l^\star \text{ if } \Lambda_l \leq \xi < \Lambda_0, \\ \mathbf{U}_r^\star \text{ if } \Lambda_0 \leq \xi < \Lambda_r, \\ \mathbf{U}_r \text{ if } \Lambda_r \leq \xi, \end{cases}$$

where $\xi = \frac{x_\mathbf{n}}{t}$.
Λ_l, Λ_0 and Λ_r are the wave speeds.

$x - t$ diagram

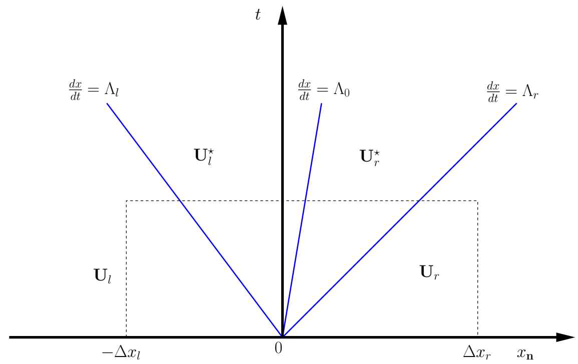

Intermediate states

$$\mathbf{U}_s^\star = \begin{pmatrix} \rho_s^\star \\ \rho_s^\star v_{\mathbf{n},s}^\star \\ \rho_s^\star \mathbf{v}_{t,s}^\star \\ \rho_s^\star e_s^\star \end{pmatrix}, \text{ for } s = l, r.$$

Intermediate fluxes

$$\mathbf{F}_{\mathbf{n},s}^\star = v_{\mathbf{n},s}^\star \mathbf{U}_s^\star + \begin{pmatrix} 0 \\ p_s^\star \\ \mathbf{0} \\ p_s^\star \mathbf{v}_{\mathbf{n},s}^\star \end{pmatrix}, \text{ for } s = l, r.$$

Characterization of the Riemann solver

Computation of $\mathbf{U}_s^\star$ and $\mathbf{F}_{\mathbf{n},s}^\star$ for $s = l, r$

- Write the conservation relations across Λ_s-waves

$$
\begin{aligned}
(\mathcal{RH}_l) &\quad -\Lambda_l(\mathbf{U}_l^\star - \mathbf{U}_l) + \mathbf{F}_{\mathbf{n},l}^\star - \mathbf{F}_{\mathbf{n},l} = \mathbf{0},\\
(\mathcal{RH}_r) &\quad -\Lambda_r(\mathbf{U}_r - \mathbf{U}_r^\star) + \mathbf{F}_{\mathbf{n},r} - \mathbf{F}_{\mathbf{n},r}^\star = \mathbf{0}.
\end{aligned}
$$

- Assume Λ_l, Λ_0 and Λ_r are given parameters
- There are $2d + 6$ scalar unknowns for $2d + 4$ scalar equations
- We have multiple choices to close this system of equations!
  - We choose to impose $v_{\mathbf{n},l}^\star = v_{\mathbf{n},r}^\star = v_{\mathbf{n}}^\star$, which is a quite natural choice
  - We decide to keep $p_l^\star \neq p_r^\star$, which is rather unusual!
  - Refer to Alessia Del Grosso talk [6A-01] Tuesday 4:30 pm for an other choice
- We arrive at $2d + 5$ scalar unknows for $2d + 4$ scalar equations
- **This allows us to consider $v_{\mathbf{n}}^\star$ as a parameter**

Characterization of the Riemann solver

Computation of $\mathbf{U}_s^\star$ and $\mathbf{F}_{\mathbf{n},s}^\star$ for $s = l, r$

Replacing $\mathbf{F}_{\mathbf{n},s} = \mathbf{v}_{\mathbf{n},s}\mathbf{U}_s + \mathbf{L}_s$ and $\mathbf{F}_{\mathbf{n},s}^\star = \mathbf{v}_{\mathbf{n}}^\star\mathbf{U}_s^\star + \mathbf{L}_s^\star$ into $(\mathcal{RH}_s)$ for $s = l, r$ yields

$$
\begin{aligned}
(\mathbf{v}_{\mathbf{n}}^\star - \Lambda_l)\mathbf{U}_l^\star - (\mathbf{v}_{\mathbf{n},l} - \Lambda_l)\mathbf{U}_l + \mathbf{L}_l^\star - \mathbf{L}_l = \mathbf{0},\\
(\mathbf{v}_{\mathbf{n},r} - \Lambda_r)\mathbf{U}_r - (\mathbf{v}_{\mathbf{n}}^\star - \Lambda_r)\mathbf{U}_r^\star + \mathbf{L}_r - \mathbf{L}_r^\star = \mathbf{0}.
\end{aligned}
$$

First components boil down to

$$
\begin{aligned}
\rho_l^\star(\mathbf{v}_{\mathbf{n}}^\star - \Lambda_l) - \rho_l(\mathbf{v}_{\mathbf{n},l} - \Lambda_l) = 0, &\quad \text{for the } \Lambda_l\text{-wave},\\
\rho_r(\mathbf{v}_{\mathbf{n},r} - \Lambda_r) - \rho_r^\star(\mathbf{v}_{\mathbf{n}}^\star - \Lambda_r) = 0, &\quad \text{for the } \Lambda_r\text{-wave}.
\end{aligned}
$$

Introduction of the mass flux parameters λ_l and λ_r

$$
\begin{aligned}
\lambda_l &= \rho_l^\star(\mathbf{v}_{\mathbf{n}}^\star - \Lambda_l) = \rho_l(\mathbf{v}_{\mathbf{n},l} - \Lambda_l),\\
\lambda_r &= -\rho_r(\mathbf{v}_{\mathbf{n},r} - \Lambda_r) = -\rho_r^\star(\mathbf{v}_{\mathbf{n}}^\star - \Lambda_r).
\end{aligned}
$$

Characterization of the Riemann solver

Expression of the wave speeds

$$\boxed{\Lambda_l = \mathbf{v}_{\mathbf{n},l} - \frac{\lambda_l}{\rho_l} = \mathbf{v}_{\mathbf{n}}^\star - \frac{\lambda_l}{\rho_l^\star}},$$

$$\boxed{\Lambda_r = \mathbf{v}_{\mathbf{n}}^\star + \frac{\lambda_r}{\rho_r^\star} = \mathbf{v}_{\mathbf{n},r} + \frac{\lambda_r}{\rho_r}}.$$

Compatibility conditions

$$\lambda_l(\tau_l^\star - \tau_l) - (\mathbf{v}_{\mathbf{n}}^\star - \mathbf{v}_{\mathbf{n},l}) = 0,$$
$$\lambda_r(\tau_r^\star - \tau_r) + \mathbf{v}_{\mathbf{n}}^\star - \mathbf{v}_{\mathbf{n},r} = 0,$$

where $\tau_s = \dfrac{1}{\rho_s}$ and $\tau_s^\star = \dfrac{1}{\rho_s^\star}$.

Conservation relations $(\mathcal{RH}_l)$ and $(\mathcal{RH}_r)$ turn into

$$\lambda_l\left(\frac{\mathbf{U}_l^\star}{\rho_l^\star} - \frac{\mathbf{U}_l}{\rho_l}\right) + \mathbf{L}_l^\star - \mathbf{L}_l = \mathbf{0},$$
$$\lambda_r\left(\frac{\mathbf{U}_r^\star}{\rho_r^\star} - \frac{\mathbf{U}_r}{\rho_r}\right) - (\mathbf{L}_r^\star - \mathbf{L}_r) = \mathbf{0}.$$

Characterization of the Riemann solver

Combining compatibility conditions and conservation relations yield

$$(\mathcal{S}_l)\begin{cases}\lambda_l(\tau_l^\star - \tau_l) - (v_{\mathbf{n}}^\star - v_{\mathbf{n},l}) = 0,\\ \lambda_l(v_{\mathbf{n}}^\star - v_{\mathbf{n},l}) + p_l^\star - p_l = 0,\\ \lambda_l(\mathbf{v}_{t,l}^\star - \mathbf{v}_{t,l}) = \mathbf{0},\\ \lambda_l(e_l^\star - e_l) + p_l^\star v_{\mathbf{n}}^\star - p_l v_{\mathbf{n},l} = 0,\end{cases} \qquad (\mathcal{S}_r)\begin{cases}\lambda_r(\tau_r^\star - \tau_r) + v_{\mathbf{n}}^\star - v_{\mathbf{n},r} = 0,\\ \lambda_r(v_{\mathbf{n}}^\star - v_{\mathbf{n},r}) - (p_r^\star - p_r) = 0,\\ \lambda_r(\mathbf{v}_{t,r}^\star - \mathbf{v}_{t,r}) = \mathbf{0},\\ \lambda_r(e_r^\star - e_r) - (p_r^\star v_{\mathbf{n}}^\star - p_r v_{\mathbf{n},r}) = 0.\end{cases}$$

Comments

- This is a system of 2d $+$ 5 unknowns for 2d $+$ 4 scalar equations, hence the $v_{\mathbf{n}}^\star$ parametrization
- It remains to
  1. Ensure positivity, *e.g.* $\tau_s^\star > 0$, $\varepsilon_s^\star > 0$ and entropy stability by adapting λ_l and λ_r
  2. Express the Λ_0 wave speed
  3. Determine the interface flux to feed the Finite Volume discretization

Positivity and entropy stability conditions

Positivity of intermediate internal energies, $\varepsilon_s^\star$, and specific volumes $\tau_s^\star$

$\varepsilon_s^\star > 0$ and $\tau_s^\star > 0$ for s=l,r provided that [Chan et al., CAF 2021]

$$\lambda_l \geq \max\left(\frac{a_l}{\tau_l}, -\frac{v_{\mathbf{n}}^\star - v_{\mathbf{n},l}}{\tau_l}\right), \text{ and } \lambda_r \geq \max\left(\frac{a_r}{\tau_r}, \frac{v_{\mathbf{n}}^\star - v_{\mathbf{n},r}}{\tau_r}\right).$$

Entropy stability

$\eta_s^\star \geq \eta_s$ provided that [Chan et al., CAF 2021]

$$\lambda_s \geq \frac{a(\tau, \eta_s)}{\tau}, \text{ for } \tau \in (\tau_s, \tau_s^\star) \text{ and } s = l, r.$$

Comment: Wave speeds ordering

$$\lambda_s > 0 \text{ and } \tau_s^\star > 0 \text{ for s=l,r} \implies \Lambda_l \leq \Lambda_0 \leq \Lambda_r.$$

Determination of the Λ_0-wave speed

Writing the balance across the Λ_0-wave

Replacing $\mathbf{F}_{\mathbf{n},s}^\star = \mathbf{v}_{\mathbf{n}}^\star \mathbf{U}_s^\star + \mathbf{L}_s^\star$ for $s = l, r$ yield

$$(\mathcal{RH}_0) \quad -\Lambda_0(\mathbf{U}_r^\star - \mathbf{U}_l^\star) + \mathbf{F}_{\mathbf{n},r}^\star - \mathbf{F}_{\mathbf{n},l}^\star = (v_{\mathbf{n}}^\star - \Lambda_0)(\mathbf{U}_r^\star - \mathbf{U}_l^\star) + \mathbf{L}_r^\star - \mathbf{L}_l^\star.$$

To simplify the right-hand side, we express the Λ_0-wave speed as

$$\boxed{\Lambda_0 = v_{\mathbf{n}}^\star}.$$

Final expression of the balance across the Λ_0-wave

$$(\mathcal{RH}_0) \quad -\Lambda_0(\mathbf{U}_r^\star - \mathbf{U}_l^\star) + \mathbf{F}_{\mathbf{n},r}^\star - \mathbf{F}_{\mathbf{n},l}^\star = \mathbf{L}_r^\star - \mathbf{L}_l^\star = (p_r^\star - p_l^\star)\begin{pmatrix} 0 \\ 1 \\ \mathbf{0} \\ v_{\mathbf{n}}^\star \end{pmatrix}.$$

This is not a conservation relation since *a priori* $p_r^\star \neq p_l^\star$.

Interface flux

Left and right-sided interface fluxes [Harten *et al.*, SIAM 1983]

$$\mathbf{F}_{\mathbf{n}}^{-} = \mathbf{F}_{\mathbf{n},l} - \int_{-\infty}^{0} [\mathbf{W}(\mathbf{U}_l, \mathbf{U}_r, \xi) - \mathbf{U}_l]\,\mathrm{d}\xi, \quad \mathbf{F}_{\mathbf{n}}^{+} = \mathbf{F}_{\mathbf{n},r} + \int_{0}^{+\infty} [\mathbf{W}(\mathbf{U}_l, \mathbf{U}_r, \xi) - \mathbf{U}_r]\,\mathrm{d}\xi.$$

Substituting the expression of our simple approximate Riemann solver leads to

$$\begin{aligned}
\mathbf{F}_{\mathbf{n}}^{-} &= \mathbf{F}_{\mathbf{n},l} - \Lambda_l^{-}(\mathbf{U}_l^{\star} - \mathbf{U}_l) - \Lambda_0^{-}(\mathbf{U}_r^{\star} - \mathbf{U}_l^{\star}) - \Lambda_r^{-}(\mathbf{U}_r - \mathbf{U}_r^{\star}),\\
\mathbf{F}_{\mathbf{n}}^{+} &= \mathbf{F}_{\mathbf{n},r} - \Lambda_l^{+}(\mathbf{U}_l^{\star} - \mathbf{U}_l) - \Lambda_0^{+}(\mathbf{U}_r^{\star} - \mathbf{U}_l^{\star}) - \Lambda_r^{+}(\mathbf{U}_r - \mathbf{U}_r^{\star}),
\end{aligned}$$

where for $x \in \mathbb{R}$ we define $x^{-} = \frac{1}{2}(|x| - x)$ and $x^{+} = \frac{1}{2}(|x| + x)$.

Jump between the right and the left-sided interface fluxes

$$\mathbf{F}_{\mathbf{n}}^{+} - \mathbf{F}_{\mathbf{n}}^{-} = \mathbf{F}_{\mathbf{n},r} - \mathbf{F}_{\mathbf{n},l} - \Lambda_l(\mathbf{U}_l^{\star} - \mathbf{U}_l) - \Lambda_0(\mathbf{U}_r^{\star} - \mathbf{U}_l^{\star}) - \Lambda_r(\mathbf{U}_r - \mathbf{U}_r^{\star}).$$

The $(\mathcal{HLL})$ consistency condition holds true iff $\mathbf{F}_{\mathbf{n}}^{+} - \mathbf{F}_{\mathbf{n}}^{-} = \mathbf{0}$.

Interface flux

Recalling $(\mathcal{RH}_l)$, $(\mathcal{RH}_0)$ and $(\mathcal{RH}_r)$

$$(\mathcal{RH}_l) \quad -\Lambda_l(\mathbf{U}_l^{\star} - \mathbf{U}_l) + \mathbf{F}_{\mathbf{n},l}^{\star} - \mathbf{F}_{\mathbf{n},l} = \mathbf{0},$$

$$(\mathcal{RH}_0) \quad -\Lambda_0(\mathbf{U}_r^{\star} - \mathbf{U}_l^{\star}) + \mathbf{F}_{\mathbf{n},r}^{\star} - \mathbf{F}_{\mathbf{n},l}^{\star} = \mathbf{L}_r^{\star} - \mathbf{L}_l^{\star} = (p_r^{\star} - p_l^{\star}) \begin{pmatrix} 0 \\ 1 \\ \mathbf{0} \\ v_{\mathbf{n}}^{\star} \end{pmatrix}$$

$$(\mathcal{RH}_r) \quad -\Lambda_r(\mathbf{U}_r - \mathbf{U}_r^{\star}) + \mathbf{F}_{\mathbf{n},r} - \mathbf{F}_{\mathbf{n},r}^{\star} = \mathbf{0}.$$

Jump between the left and right-sided interface fluxes

Summing $(\mathcal{RH}_l)$, $(\mathcal{RH}_0)$ and $(\mathcal{RH}_r)$ leads to

$$\mathbf{F}_{\mathbf{n}}^{+} - \mathbf{F}_{\mathbf{n}}^{-} = \mathbf{L}_r^{\star} - \mathbf{L}_l^{\star} = (p_r^{\star} - p_l^{\star}) \begin{pmatrix} 0 \\ 1 \\ \mathbf{0} \\ v_{\mathbf{n}}^{\star} \end{pmatrix}.$$

Conservation holds true in the classical sense if and only if $p_r^{\star} - p_l^{\star} = 0$.

Interface flux

Jump between the intermediate pressures

Summing the the momentum equation of $(\mathcal{S}_l)$ and $(\mathcal{S}_r)$ yields

$$p_r^\star - p_l^\star = (\lambda_l + \lambda_r)(v_{\mathbf{n}}^\star - \overline{v}_{\mathbf{n},lr}) \text{ where } \overline{v}_{\mathbf{n},lr} = \frac{\lambda_l v_{\mathbf{n},l} + \lambda_r v_{\mathbf{n},r}}{\lambda_l + \lambda_r} - \frac{(p_r - p_l)}{\lambda_r + \lambda_l},$$

which is the approximation of normal component of the velocity interface.

Alternative for the parameter $v_{\mathbf{n}}^\star$ and the interface flux

- Either $v_{\mathbf{n}}^\star = \overline{v}_{\mathbf{n}}$, then the Riemann solver is consistent with (RP) and it induces a classical face-based conservative Finite Volume scheme characterized by the unique interface flux $\mathbf{F}_{\mathbf{n}}^+ = \mathbf{F}_{\mathbf{n}}^-$;
- Or $v_{\mathbf{n}}^\star \neq \overline{v}_{\mathbf{n}}$, then the Riemann solver is not consistent with (RP) and it does not induce a conservative Finite Volume scheme in the classical sense since $\mathbf{F}_{\mathbf{n}}^+ \neq \mathbf{F}_{\mathbf{n}}^-$.

How to compute $v_{\mathbf{n}}^\star$ and restore the conservation property when $\mathbf{F}_{\mathbf{n}}^+ \neq \mathbf{F}_{\mathbf{n}}^-$?

Subface-based Finite Volume discretization

Assumptions and notations

- Polyhedral tessellation with cells ω_c
- $\mathcal{P}(c)$ set of vertices p of ω_c
- Faces partition into **subfaces**
- Quadrangular subface: $\{\mathbf{x}_p, \mathbf{x}_{pcf,1}, \mathbf{x}_{cf}, \mathbf{x}_{pcf,2}\}$
- $\mathcal{SF}(pc)$ set of subfaces related to p and c
- Subface partition into triangles $T_{pcf,1}$ and $T_{pcf,2}$
- $\mathbf{n}_{pcf}$: outward unit normal to the subface

$$A_{pcf}\mathbf{n}_{pcf} = |T_{pcf,1}|\mathbf{n}_{pcf,1} + |T_{pcf,2}|\mathbf{n}_{pcf,2}$$

Hexaedral cell

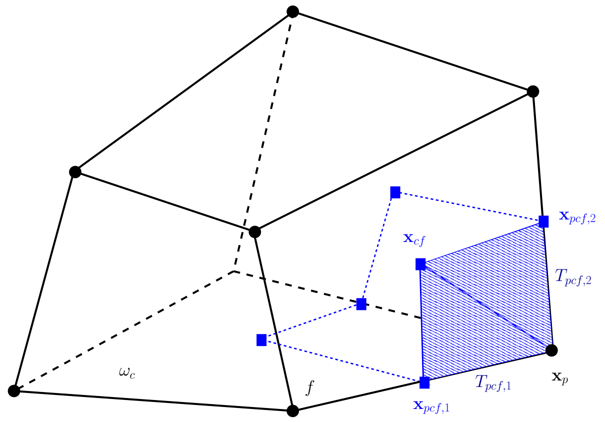

Subface-based FV discretization

$$\mathbf{U}_c^{n+1} - \mathbf{U}_c^n + \frac{\Delta t}{|\omega_c|} \sum_{p \in \mathcal{P}(c)} \sum_{f \in \mathcal{SF}(pc)} A_{pcf} \overline{\mathbf{F}}_{pcf} = \mathbf{0},$$

Here, $\overline{\mathbf{F}}_{pcf}$ is the **subface flux** attached to the subface f and the corner pc.

Subface flux approximation

Riemann problem

$$\begin{cases} \dfrac{\partial \mathbf{U}}{\partial t} + \dfrac{\partial \mathbf{F}_{\mathbf{n}_{pcf}}}{\partial x_{\mathbf{n}_{pcf}}} = \mathbf{0}, \\ \text{where } \mathbf{F}_{\mathbf{n}_{pcf}} = \mathbb{F}(\mathbf{U})\mathbf{n}_{pcf}. \\ \mathbf{U}(x_{\mathbf{n}_{pcf}}, 0) = \begin{cases} \mathbf{U}_c^n \text{ if } x_{\mathbf{n}_{pcf}} < 0, \\ \mathbf{U}_d^n \text{ if } x_{\mathbf{n}_{pcf}} \geq 0. \end{cases} \end{cases}$$

Parametrized Riemann solver

$$\mathbf{W} = \mathbf{W}_{pcf}(\mathbf{U}_c^n, \mathbf{U}_d^n, v^\star_{\mathbf{n}_{pcf}}, \xi)$$

Interface between ω_c and ω_d

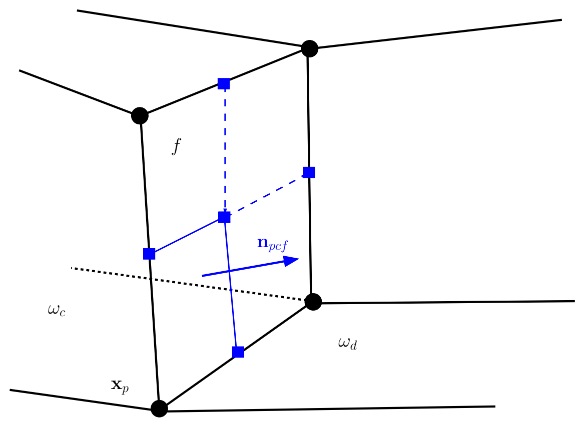

Subface flux approximation

$$\overline{\mathbf{F}}_{pcf} = \mathbf{F}^-_{\mathbf{n}_{pcf}} = \mathbf{F}^n_{\mathbf{n}_{pcf},c} - \int_{-\infty}^{0} \left[\mathbf{W}_{pcf}(\mathbf{U}_c^n, \mathbf{U}_d^n, v^\star_{\mathbf{n}_{pcf}}, \xi) - \mathbf{U}_c^n \right] \mathrm{d}\xi.$$

A priori $\overline{\mathbf{F}}_{pcf} \neq \overline{\mathbf{F}}_{pdf}$ and thus the FV scheme is not conservative!

Convex combination property

Expressing $\mathbf{U}_c^{n+1}$ in terms of the intermediate states

Recalling the expression of the left-sided flux

$$\mathbf{F}_{pcf} = \mathbf{F}^n_{\mathbf{n}_{pcf},c} - \Lambda^-_{l,f}(\mathbf{U}^\star_{l,f} - \mathbf{U}^n_c) - \Lambda^-_{0,f}(\mathbf{U}^\star_{r,f} - \mathbf{U}^\star_{l,f}) - \Lambda^-_{r,f}(\mathbf{U}^n_d - \mathbf{U}^\star_{r,f}).$$

Substituting it into the FV scheme and rearranging leads to

$$\mathbf{U}_c^{n+1} = \left[1 - \frac{\Delta t}{|\omega_c|} \sum_{p \in \mathcal{P}(c)} \sum_{f \in \mathcal{SF}(pc)} A_{pcf} \Lambda^-_{l,f}\right] \mathbf{U}_c^n + \frac{\Delta t}{|\omega_c|} \sum_{p \in \mathcal{P}(c)} \sum_{f \in \mathcal{SF}(pc)} A_{pcf} \left(\Lambda^-_{l,f} - \Lambda^-_{0,f}\right) \mathbf{U}^\star_{l,f}$$
$$+ \frac{\Delta t}{|\omega_c|} \sum_{p \in \mathcal{P}(c)} \sum_{f \in \mathcal{SF}(pc)} A_{pcf} \left[\left(\Lambda^-_{0,f} - \Lambda^-_{r,f}\right) \mathbf{U}^\star_{r,f} + \Lambda^-_{r,f} \mathbf{U}^n_d \right].$$

$\mathbf{U}_c^{n+1}$ convex combination of the intermediate states if

$$\Delta t \leq \min_c \Delta t_c, \text{ where } \Delta t_c = \frac{|\omega_c|}{\sum_{p \in \mathcal{P}(c)} \sum_{f \in \mathcal{SF}(pc)} A_{pcf} \Lambda^-_{l,f}}.$$

Conservation property of the FV scheme

The Finite Volume scheme is conservative iff

$$\sum_c |\omega_c|(\mathbf{U}_c^{n+1} - \mathbf{U}_c^n) = \mathbf{0} \Longleftrightarrow \sum_c \sum_{p\in\mathcal{P}(c)} \sum_{f\in\mathcal{SF}(pc)} A_{pcf}\overline{\mathbf{F}}_{pcf} = \mathbf{0},$$

$$\Longleftrightarrow \sum_p \sum_{c\in\mathcal{C}(p)} \sum_{f\in\mathcal{SF}(pc)} A_{pcf}\overline{\mathbf{F}}_{pcf} = \mathbf{0},$$

where $\mathcal{C}(p)$ is the set of cells sharing point p.

The node-based conservation

$$\sum_{c\in\mathcal{C}(p)} \sum_{f\in\mathcal{SF}(pc)} A_{pcf}\overline{\mathbf{F}}_{pcf} = \mathbf{0},$$

$$\sum_{f\in\mathcal{SF}(p)} \sum_{c\in\mathcal{C}(f)} A_{pcf}\overline{\mathbf{F}}_{pcf} = \mathbf{0},$$

$\mathcal{SF}(p)$ set of subfaces impinging at p,

$\mathcal{C}(f)$ set of cells sharing sufbace f.

The node-based condition (NBC)

$$\sum_{f\in\mathcal{SF}(p)} A_{pf}(\mathbf{F}^+_{\mathbf{n}_{pf}} - \mathbf{F}^-_{\mathbf{n}_{pf}}) = \mathbf{0},$$

$\mathbf{F}^-_{\mathbf{n}_{pf}}$ left-sided flux w.r.t. $\mathbf{n}_{pf}$,

$\mathbf{F}^+_{\mathbf{n}_{pf}}$ right-sided flux w.r.t. $\mathbf{n}_{pf}$.

Conservation property of the FV scheme

Grid fragment at point p

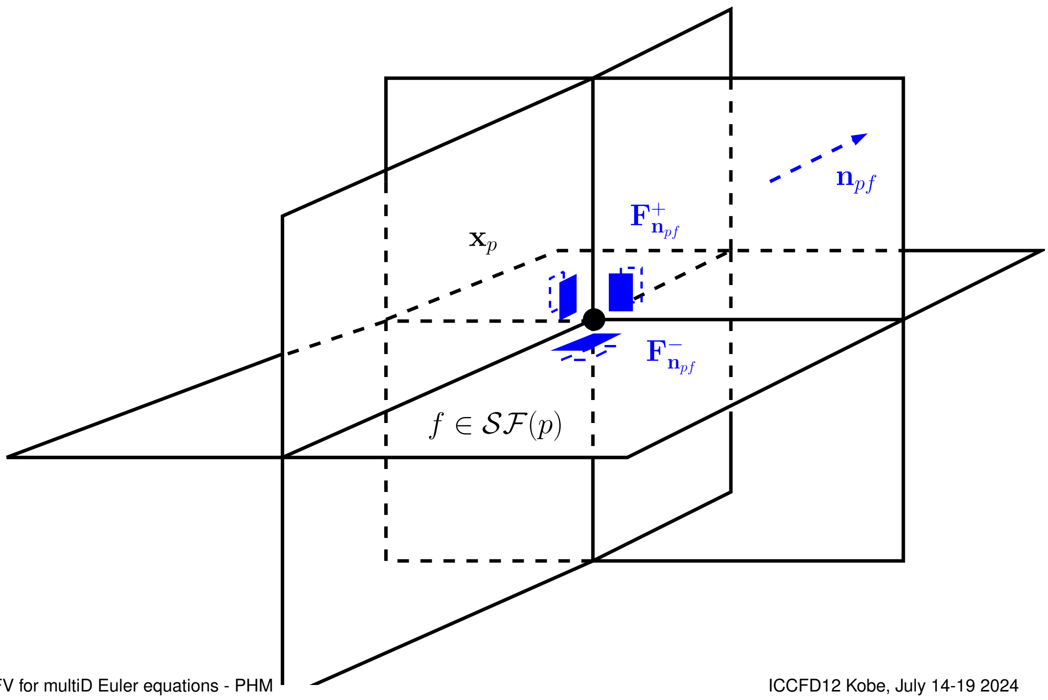

Conservation property of the FV scheme

Substituting the expression of $\mathbf{F}^{+}_{\mathbf{n}_{pf}} - \mathbf{F}^{-}_{\mathbf{n}_{pf}}$ into (NBC) leads to

$$\mathbf{F}^{+}_{\mathbf{n}_{pf}} - \mathbf{F}^{-}_{\mathbf{n}_{pf}} = (\lambda_{l,pf} + \lambda_{r,pf}) \left(v^{\star}_{\mathbf{n}_{pf}} - \overline{v}_{\mathbf{n}_{pf},lr} \right) \begin{pmatrix} 0 \\ 1 \\ \mathbf{0} \\ v^{\star}_{\mathbf{n}_{pf}} \end{pmatrix}.$$

We have $|\mathcal{SF}(p)|$ scalar unknowns for only d+1 scalar equations!

Closure assumption on the $v^{\star}_{\mathbf{n}_{pf}}$ parameter

$$\boxed{v^{\star}_{\mathbf{n}_{pf}} = \mathbf{v}_p \cdot \mathbf{n}_{pf}, \ \forall f \in \mathcal{SF}(p).}$$

This introduces the nodal velocity $\mathbf{v}_p$, which shall be computed from the NBC.

Conservation property of the FV scheme

The nodal solver

Substituting the expression of $v^{\star}_{\mathbf{n}_{pf}}$ in (NBC) turns it into

$$\sum_{f \in \mathcal{SF}(p)} A_{pf}(\lambda_{l,pf} + \lambda_{r,pf})(\mathbf{n}_{pf} \otimes \mathbf{n}_{pf})\mathbf{v}_p = \sum_{f \in \mathcal{SF}(p)} A_{pf}(\lambda_{l,pf} + \lambda_{l,pf})\overline{v}_{\mathbf{n}_{pf}} \mathbf{n}_{pf},$$

$$\text{where } \overline{v}_{\mathbf{n}_{pf}} = \frac{\lambda_{l,pf} v_{\mathbf{n},l,pf} + \lambda_{r,pf} v_{\mathbf{n},r,pf}}{\lambda_{l,pf} + \lambda_{r,pf}} - \frac{(p_{r,pf} - p_{r,pf})}{\lambda_{r,pf} + \lambda_{l,pf}}$$

- This system admits a unique solution which provides an approximation of the nodal velocity $\mathbf{v}_p$
- **It coincides with the one constructed for Lagrangian hydrodynamics [PHM, JCP 2009]**
- It's not a suprise since this Riemann solver has Lagrangian roots [Gallice *et al.*, JCP 2022]
- This allows to compute the intermediate states and fluxes of the Riemann solver

Two types of FV scheme

Classical face-based FV

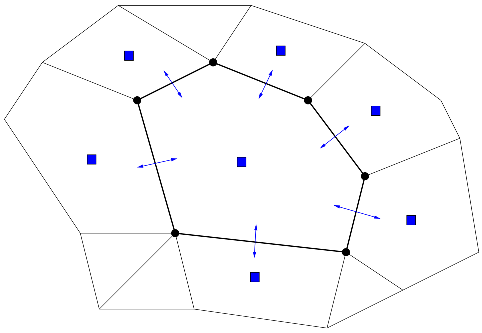

Unconventional subface-based FV

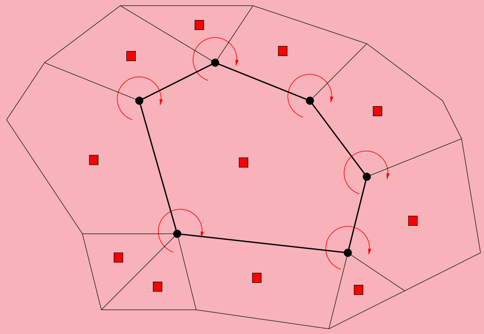

- Classical face-based FV method: interface flux computed from the classical approximate Riemann solver depending on the left and right states on both sides of the interface, hence the name **Two-point scheme**
- Unconventional subface-based FV method: subface flux computed from the nodal solver depending on all the states surrounding the node, hence the name **Multipoint scheme**

3D extension of odd-even decoupling test [Quirk, IJNMF 1994]

Test case definition

- Assess the sensitivity of numerical methods to infinitesimal perturbations
- Planar shock wave propagation over a perturbed Cartesian grid
- Computational domain is $\Omega = \{(x, y, z) \in [0, 800] \times [-10, 10] \times [-10, 10]\}$
- Cartesian grid $800 \times 20 \times 20$
- Perturbation of the centerline $y = 0$ and $z = 0$

$$\tilde{\mathbf{x}}_p = \mathbf{x}_p + a_0 \begin{pmatrix} 0 \\ \cos(\phi) \\ \sin(\phi) \end{pmatrix},$$

where a_0 is the amplitude of the pertubation and ϕ the angle defined by $\phi = (\mathbf{x}_p \cdot \mathbf{e}_x)\frac{\pi}{2}$.

3D extension of odd-even decoupling test [Quirk, IJNMF 1994]

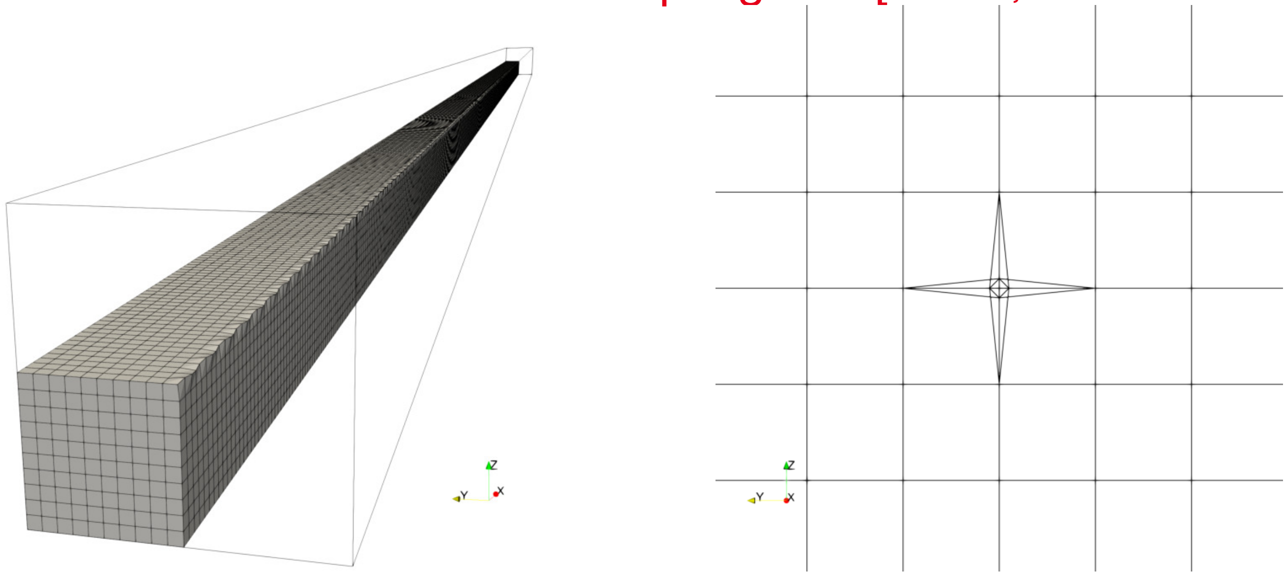

(a) Grid bottom left quadrant. (b) Zoom at the centerline.

Figure 1: Grid fragments for a perturbation of amplitude $a_0 = 0.1$.

3D extension of odd-even decoupling test [Quirk, IJNMF 1994]

Set up

- Mach 6 right-going shock wave
- Initial state $(\rho^0, \mathbf{v}, p^0, \gamma) = (1, \mathbf{0}, 1, \frac{7}{5})$
- Rankine-Hugoniot relations provides the inflow state

$$u_{\text{shock}} = \text{Ma}\sqrt{\gamma}, \quad \rho_\infty = \frac{(\gamma+1)\text{Ma}^2}{(\gamma-1)\text{Ma}^2+2}, \quad u_\infty = u_{\text{shock}}\frac{2(\text{Ma}^2-1)}{(\gamma+1)\text{Ma}^2}, \quad p_\infty = \frac{2\gamma\text{Ma}^2-(\gamma-1)}{(\gamma+1)},$$

  where Ma denotes the Mach number
- Final time: $t_{\text{final}} = 50$
- Exact solution: 1D shock wave propagating at speed u_{shock} in the x-direction

Numerical solution should remain uniform regardless the amplitude of the perturbation

3D extension of odd-even decoupling test [Quirk, IJNMF 1994]

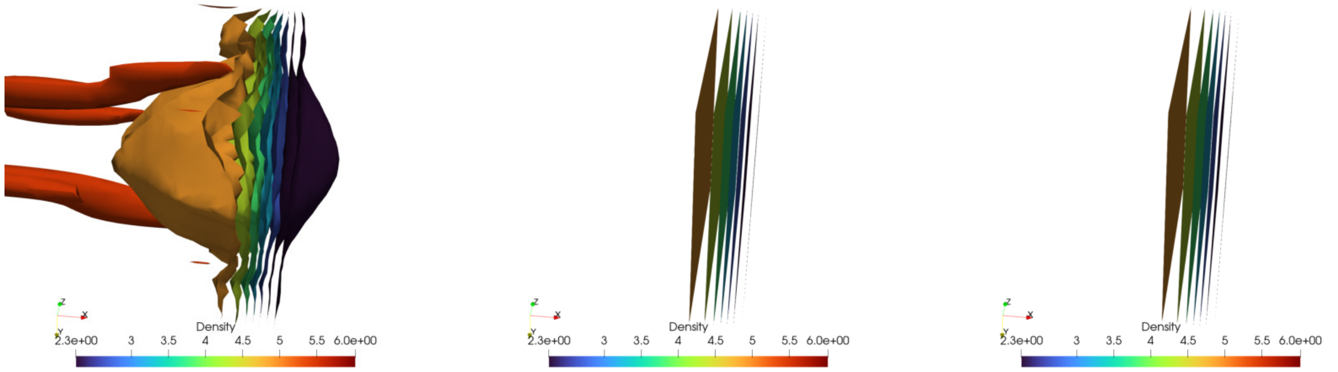

(a) 2-point scheme. (b) Modified 2-point scheme. (c) Multi-point scheme.

Figure 2: Density isosurfaces viewed from aside at time $t_{final} = 50$ with $a_0 = 10^{-9}$.

Sedov problem [Kamm *et al.*, LANL 2007]

Test case set up

- $(x, y, z) \in [-1.2, 1.2]^3$
- Set up

$$(\rho_0, \mathbf{v}_0, p_0) = (1, \mathbf{0}, 10^{-6})$$
$$p_{\text{origin}} = (\gamma - 1)\rho_{\text{origin}} \frac{\mathcal{E}_0}{V_{\text{origin}}},$$
$$\mathcal{E}_0 = 0.851072, \text{ energy release.}$$

- Hexaedral grid: 64x64x64
- Point-blast with a self-similar solution
- $R_{\text{shock}} = 1$ at $t_{\text{stopping}} = 1$

Scattered◇ plot of density (hex.)

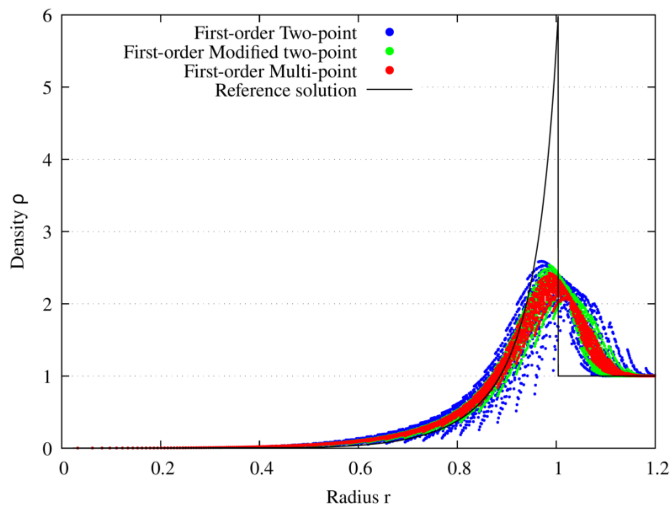

◇ Scattered plot: density in all the cells with respect to the cell center radius.

Sedov problem [Kamm *et al.*, LANL 2007]

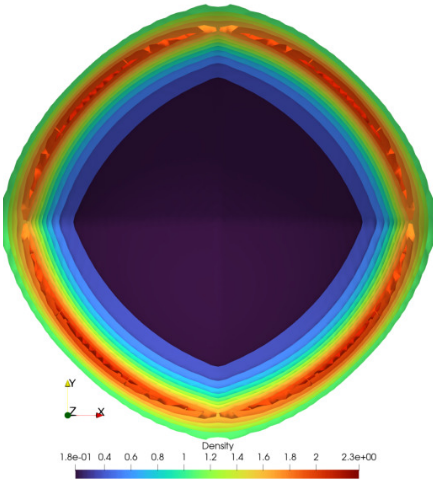

(a) 2-point scheme.

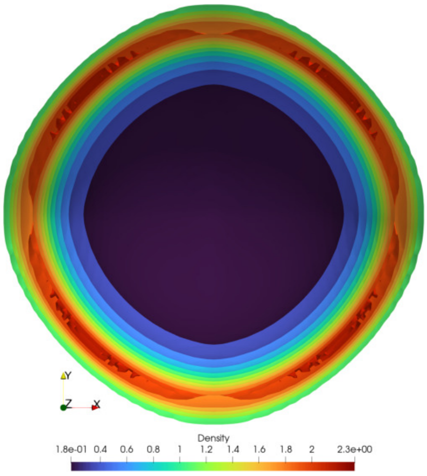

(b) Modified 2-point scheme.

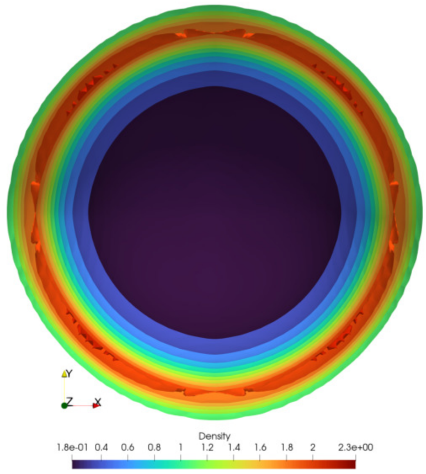

(c) Multipoint scheme.

Figure 3: Sedov test case on the Cartesian grid made of 64^3 hexaedras. Density contours at time $t = 1$: 15 equally spaced iso surfaces over [0, 2.5]. View of the domain $z < 0$.

Blunt body test case [Candler *et al.*, AIAA 2007]

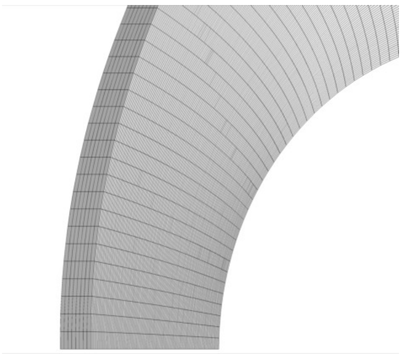

(a) Hexaedral grid.

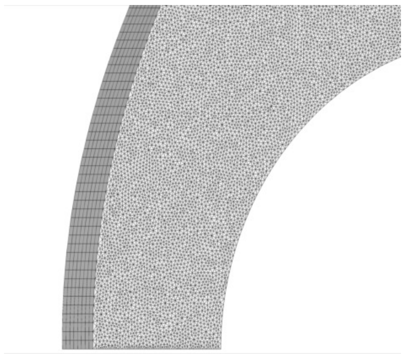

(b) Prismatic grid.

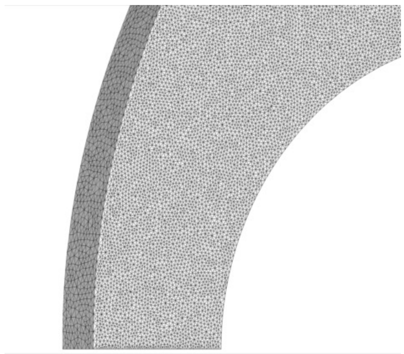

(c) Tetrahedral grid.

Figure 4: Blunt-body test case: types of grids used after [Candler, AIAA 2007].

- Mach 12 flow over a cylinder normal to the flow: singularity of the stagnation line!
- Hexaedral grid aligned with the bow shock and also a non aligned grid

Blunt body test case [Candler *et al.*, AIAA 2007]

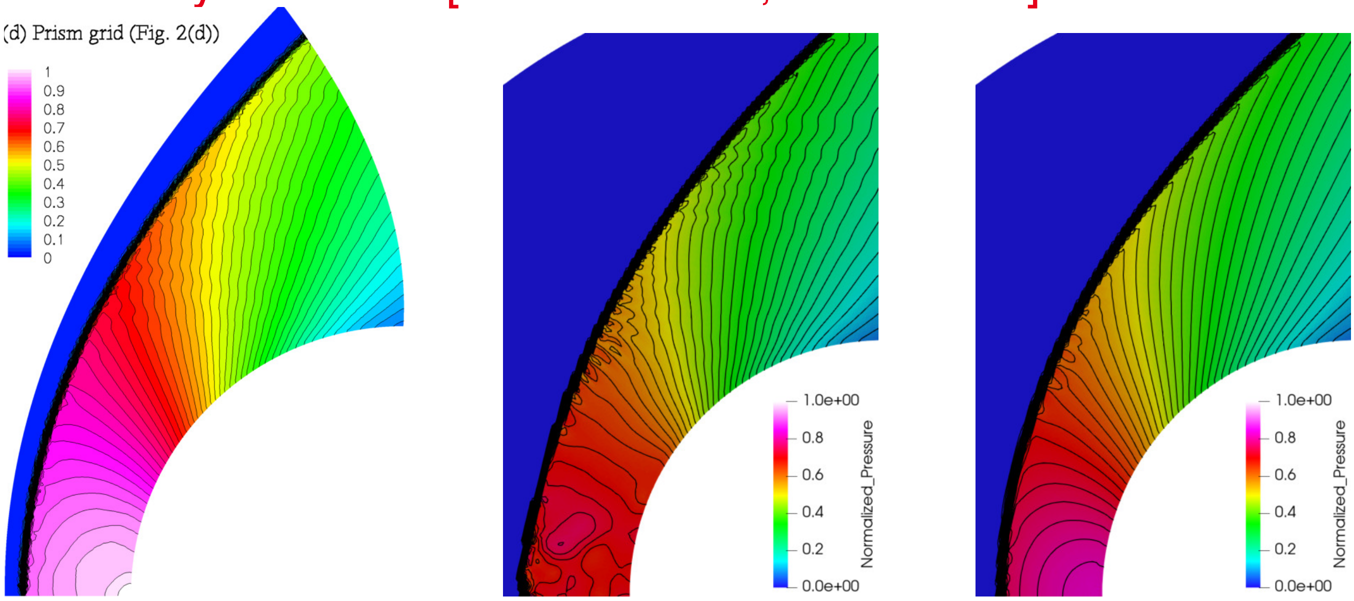

(a) US3D code. (b) Two-point. (c) Multipoint.

Figure 5: Blunt-body problem using a **prismatic grid**: Pressure contours.

Blunt body test case [Candler *et al.*, AIAA 2007]

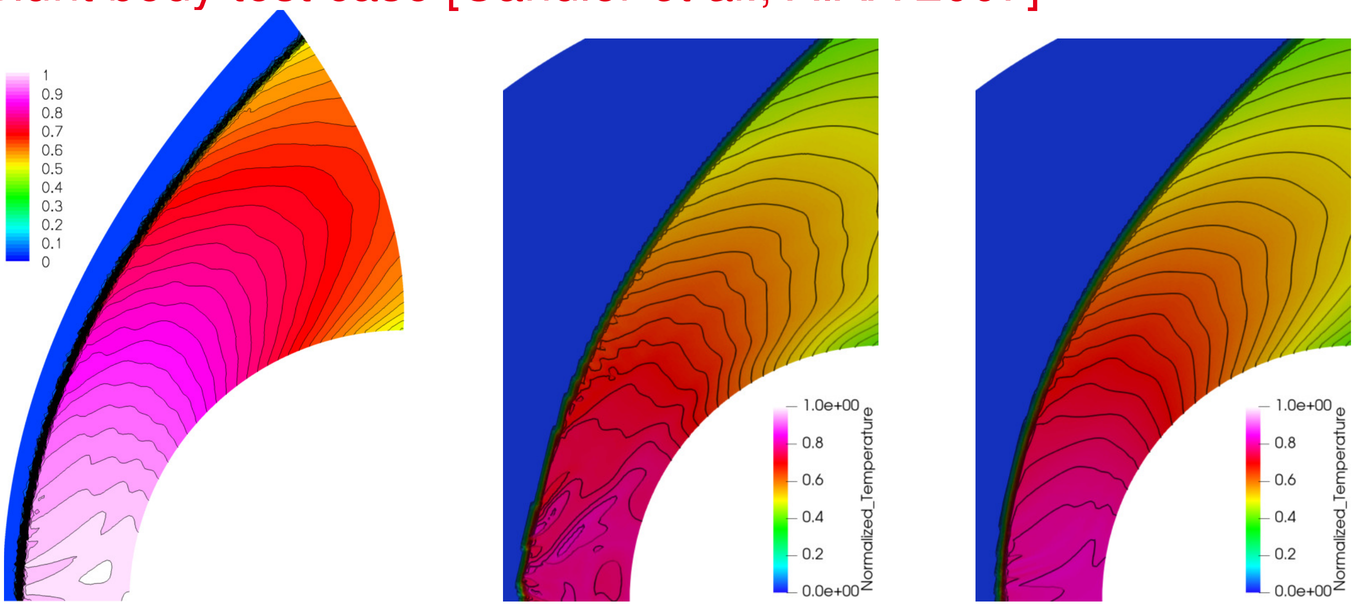

(a) US3D code. (b) Two-point. (c) Multipoint.

Figure 6: Blunt-body problem using a **prismatic grid**: Temperature contours.

Blunt body test case [Candler *et al.*, AIAA 2007](prismatic grid)

Pressure coefficient $C_p = \dfrac{p_{\text{wall}} - p_\infty}{\frac{1}{2}\rho_\infty \mathbf{v}_\infty^2}$

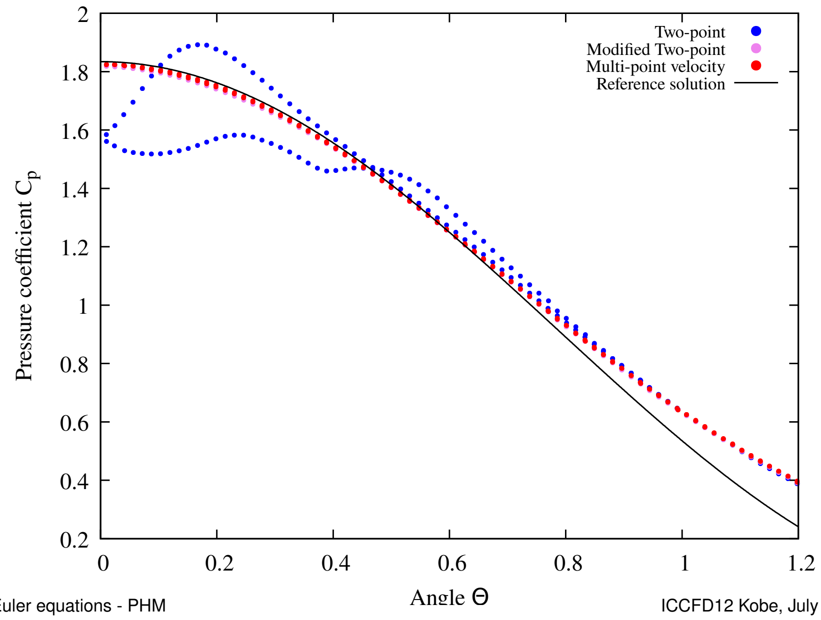

Blunt body test case [Candler *et al.*, AIAA 2007] (prismatic grid)

Density along stagnation line

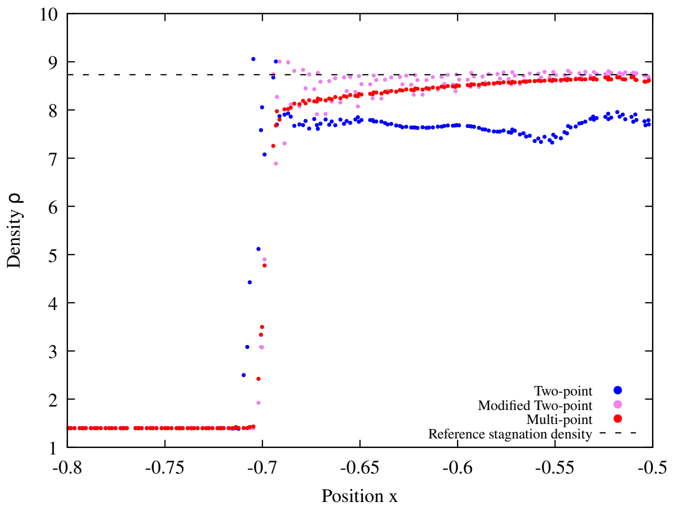

Total enthalpy along stagnation line

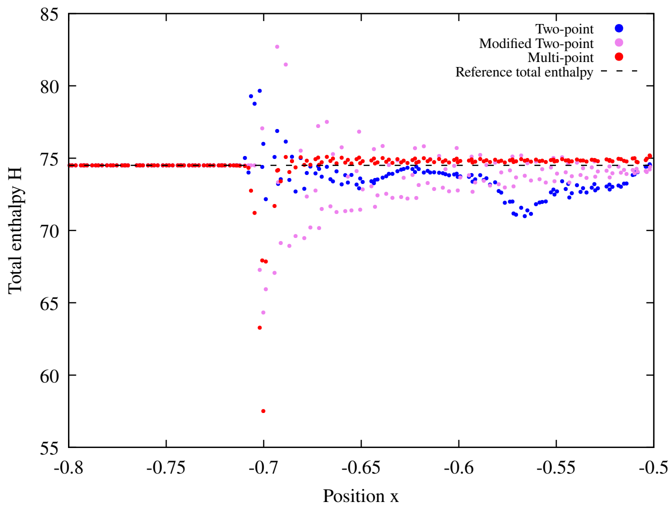

N.B.: Total enthalpy, $H = \varepsilon + \frac{p}{\rho} + \frac{1}{2}\mathbf{v}^2$, should be conserved for such a flow

Blunt body test case [Candler *et al.*, AIAA 2007]

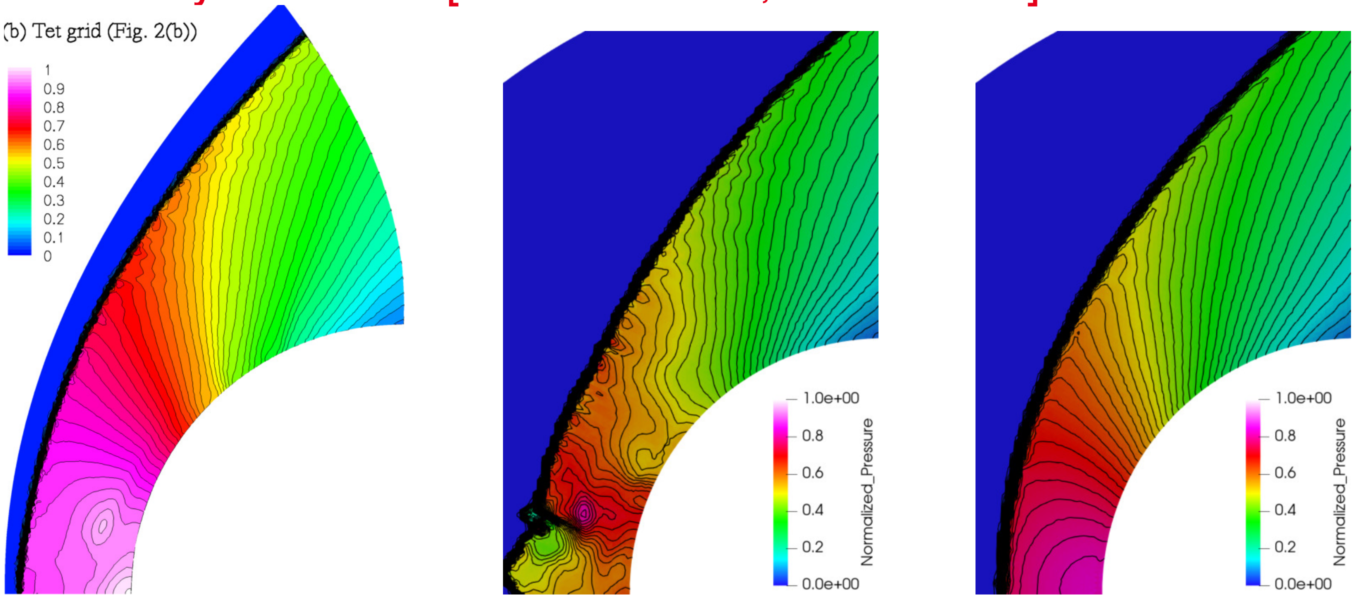

(a) US3D code. (b) Two-point. (c) Multipoint.

Figure 7: Blunt-body problem using a **tetrahedral grid**: Pressure contours.

Blunt body test case [Candler *et al.*, AIAA 2007]

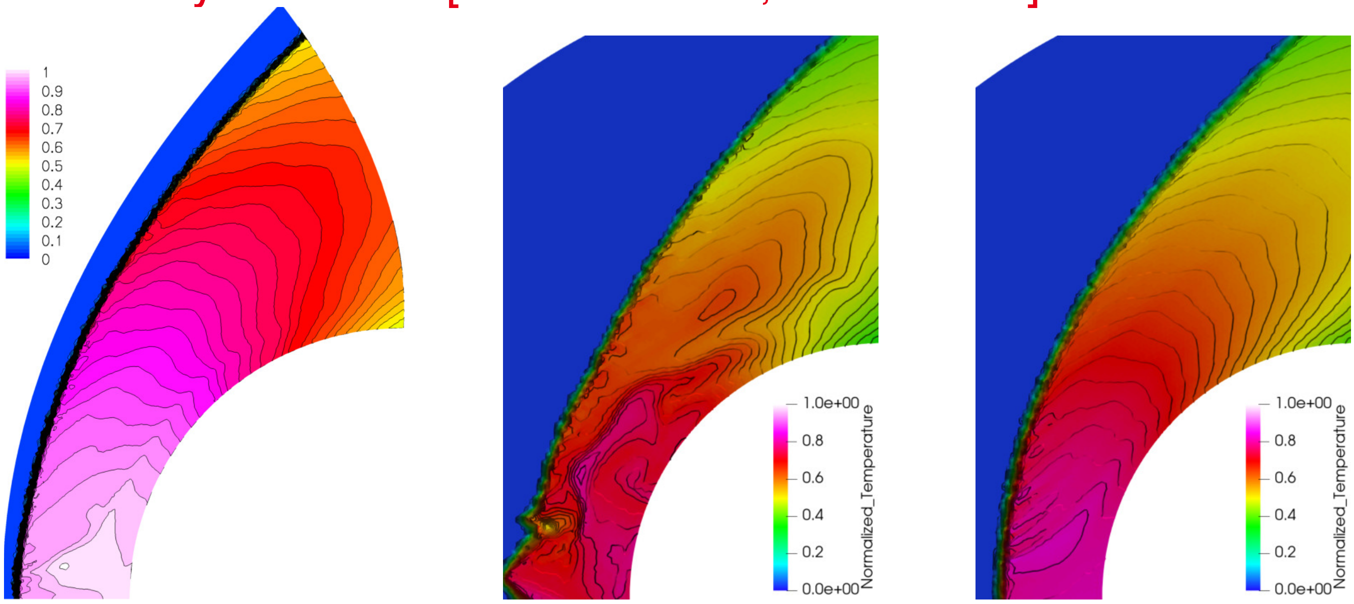

(a) US3D code. (b) Two-point. (c) Multipoint.

Figure 8: Blunt-body problem using a **tetrahedral grid**: Temperature contours.

Blunt body test case [Candler *et al.*, AIAA 2007] (tet.grid)

Pressure coefficient $C_p = \dfrac{p_{\text{wall}} - p_\infty}{\frac{1}{2}\rho_\infty \mathbf{v}_\infty^2}$

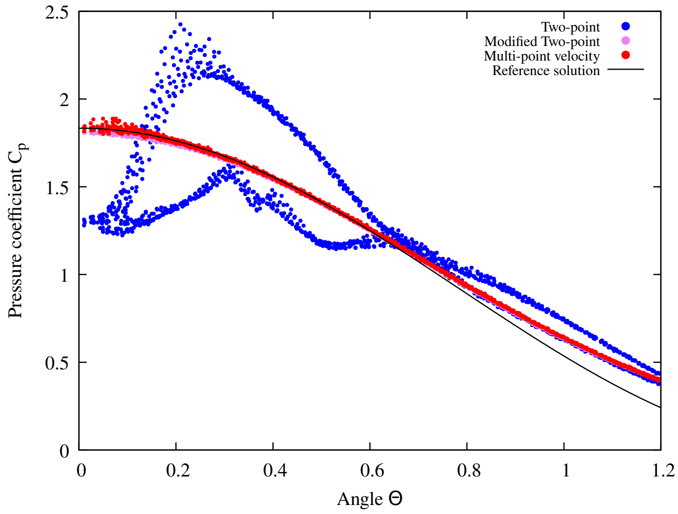

N.B.: Comparison with the modified Newtonian theory [Anderson, AIAA 2006]

Blunt body test case [Candler *et al.*, AIAA 2007] (tet. grid)

Density along stagnation line

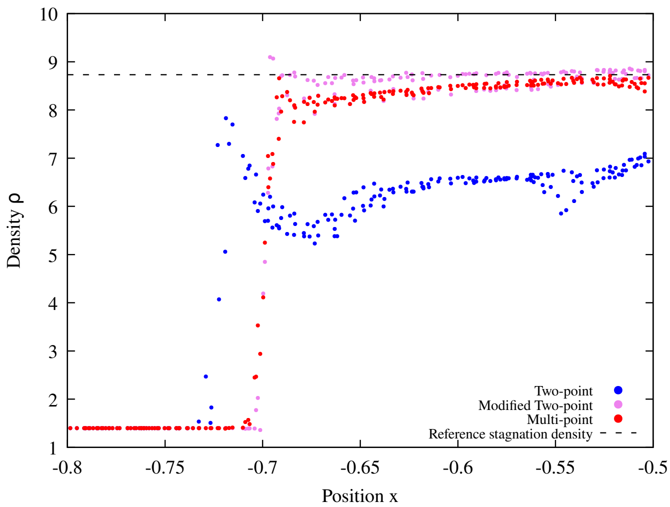

Total enthalpy along stagnation line

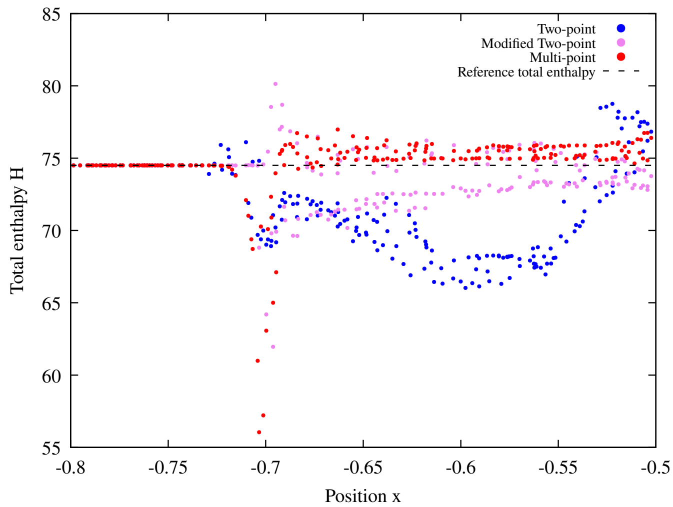

N.B.: Total enthalpy, $H = \varepsilon + \frac{p}{\rho} + \frac{1}{2}\mathbf{v}^2$, should be conserved for such a flow

PRE-X test case [Annaloro *et al.*, ESA Conf. 2017]

Freestream conditions

Quantities	PRE-X
Mach	**25**
Altitude (km)	**73.6**
Velocity (ms^{-1})	**7205**
Density (kgm^{-3})	**5.546 10^{-5}**
Temperature (K)	**207**
Pressure (Pa)	**3.11**
Wall temperature (K)	**1500**
Angle of attack (^{o})	**40**

Grid: 6M tetrahedra (Gmsh)

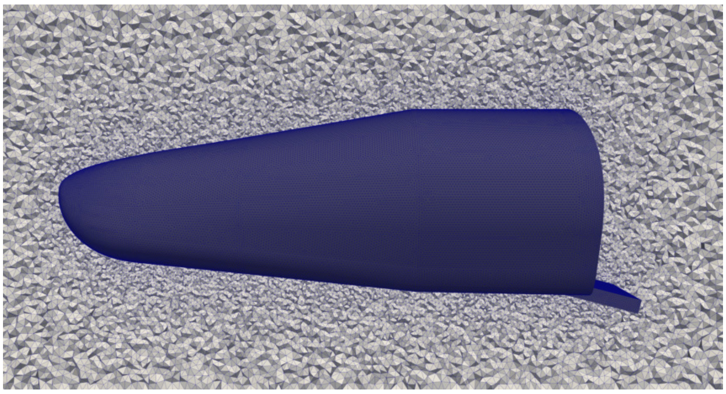

PREX test case [Annaloro *et al.*, ESA Conf. 2017]

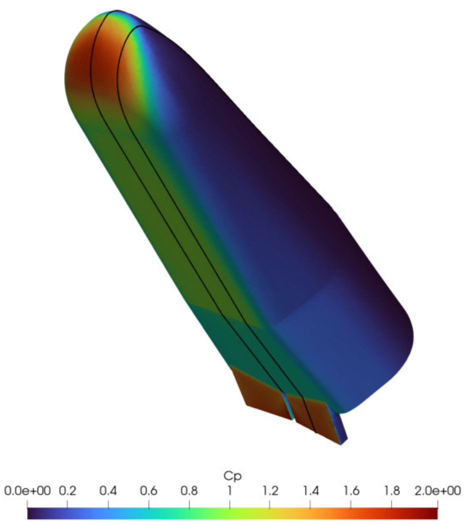

(a) Traces of $y = 0$ and $y = 0.3\,\mathrm{m}$.

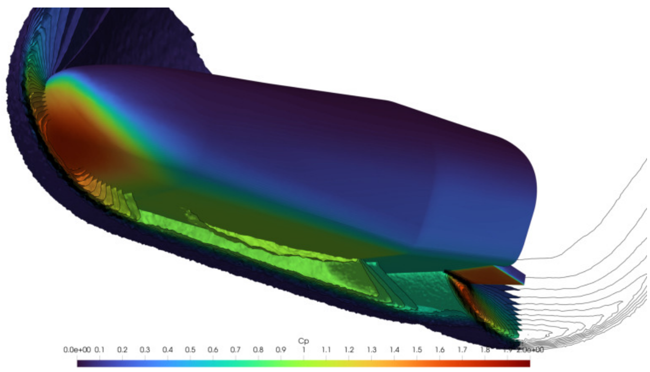

(b) Pressure iso-surfaces, multipoint.

Figure 9: Representations of the pressure field.

PREX test case [Annaloro *et al.*, ESA Conf. 2017]

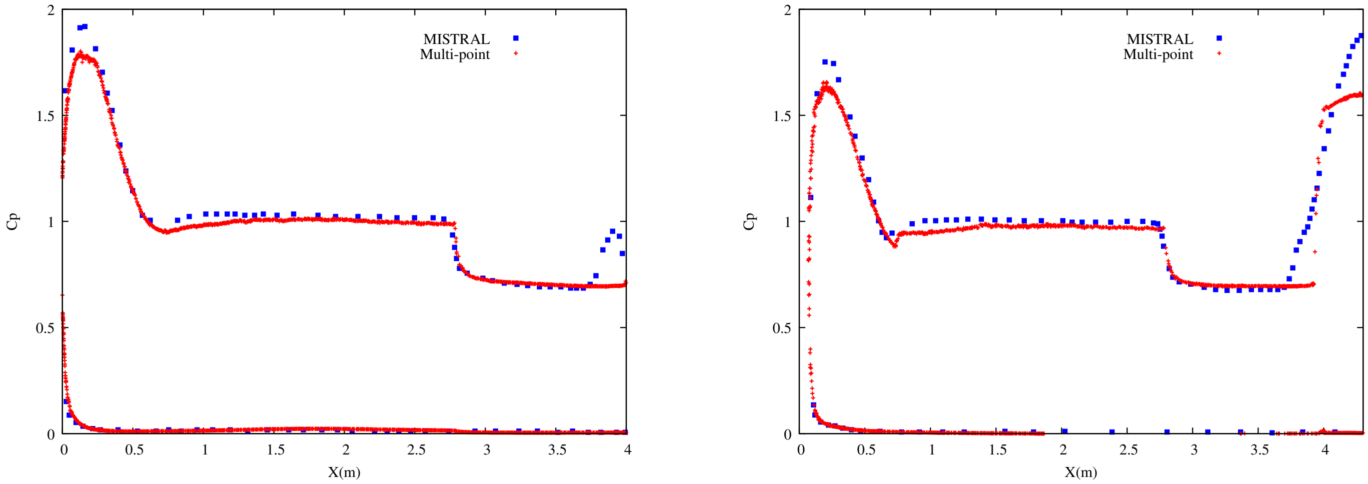

(a) Pressure coefficient along the trace of the plane $y = 0$ on the surface.

(b) Pressure coefficient along the trace of the plane $y = 0.3$ on the surface.

Figure 10: Pressure coefficient obtained by the multipoint FV scheme and the MISTRAL code, which is a multibloc structured Navier-Stokes code (R.Tech).

Conclusion and perspectives

Conclusion

- Subface-based Finite Volume scheme for Euler equations
- Subface numerical flux by means of a specific approximate Riemann solver
- **Positivity preserving method**
- **Conservation node-based condition**
- **Multipoint scheme seems to be less sensitive to numerical pathologies that plague classical two-point schemes**

Perspectives

- Investigation of the theoretical properties
- Low Mach extension $\longrightarrow$ *cf.* Alessia Del Grosso talk [6A-01] Tuesday 4:30 pm
- Entropy conservative flux utilizing Abgrall approach [Abgrall, JCP 2018]
- Time implicit discretization $\longrightarrow$ *cf.* Benoit Cossart talk [11D-02] Thursday 2:30 pm
- Viscous and heat fluxes discretization for Navier-Stokes extension extending the multipoint flux approximation introduced in [Jacq, Ph.D. 2014]

Further readings

A. Chan and G. Gallice and R. Loubère and P.-H. Maire
Positivity preserving and entropy consistent approximate Riemann solvers dedicated to the high-order MOOD-based Finite Volume discretization of Lagrangian and Eulerian gas dynamics
Computers & Fluids, 2021.

A. Del Grosso and A. Chan and G. Gallice and R. Loubère and P.-H. Maire
A well-balanced, positive, entropy-stable, and multi-dimensional-aware finite volume scheme for 2D shallow-water equations with unstructured grids
Journal of Computational Physics, 2024.

G. Gallice and A. Chan and R. Loubère and P.-H. Maire
Entropy stable and positivity preserving Godunov-type schemes for multi-dimensional hyperbolic systems on untructured grid
Journal of Computational Physics, 2022.

G. Gallice
Positive and entropy stable Godunov-type schemes for gas dynamics and MHD equations in Lagrangian or Eulerian coordinates.
Numer. Math., 94:673–713, 2003.

A. Harten and P. Lax and B. van Leer
On upstream differencing and Godunov-type schemes for hyperbolic conservation laws
SIAM Review, 25:35–61, 1983.

P. Jacq
Finite Volume methods on unstructured grids for solving anisotropic heat transfer and compressible Navier-Stokes equations
Ph.D. Thesis, Bordeaux University, 2014

R. Menikoff and B. J. Plohr
The Riemann problem for fluid flow of real materials.
Review of Modern Physics, 61:75–130, 1989.

Hypersonic flows [Anderson, AIAA 2006]

Structure of an hypersonic flow in front of blunt body

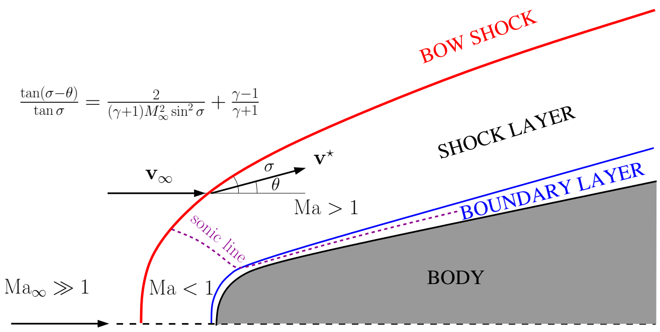

Main features of hypersonic flows in continuum regime

- Strong curved shock wave: conversion of kinetic energy into internal energy, vorticity and entropy gradients
- High temperatures flow: thermochemical processes have to be taken into account
- Thin shock layer: shock close to the body
- Viscous interaction: standard first-order boundary layer theory not valid anymore

Basic mathematical model for continuum hypersonics

Compressible Navier-Stokes equations

$$\frac{\partial \rho}{\partial t} + \nabla\cdot(\rho \mathbf{v}) = 0,$$
$$\frac{\partial}{\partial t}(\rho \mathbf{v}) + \nabla\cdot(\rho \mathbf{v}\otimes \mathbf{v}) + \nabla p = \nabla\cdot \mathbb{S},$$
$$\frac{\partial}{\partial t}(\rho e) + \nabla\cdot(\rho e \mathbf{v}) + \nabla\cdot(p\mathbf{v}) = \nabla\cdot(\mathbb{S}\mathbf{v}) - \nabla\cdot \mathbf{q}.$$

Constitutive laws

$\mathbb{S} = 2\mu\mathbb{D}_0$ and $\mathbf{q} = -\kappa\nabla\theta$,

$$\mathbb{D}_0 = \frac{1}{2}[\nabla\mathbf{v} + (\nabla\mathbf{v})^t] - \frac{1}{3}(\nabla\cdot\mathbf{v})\,\mathbb{I}_d,$$

Equation of state

Comments

- This is the basic model knowing that for hypersonic applications a larger number of equations must be solved!
- Navier-Stokes equations consists of a convective part plus a viscous-heat conducting part
- We focus on the **Finite Volume discretization** of the convective part: **the Euler equations**
- Most of the production codes for hypersonic flows rely on FV discretization: NASA (LAURA, DPLR, US3D), ONERA (CEDRE, ELSA), DLR (TAU)...

Finite Volume method for inviscid hypersonic flows

Main difficulties

- **Numerical simulation of hypersonic flows is still challenging!** [Kitamura, Springer 2020]
- Hypersonic regime exacerbates the eternal trade-off between robustness and accuracy
  - Sufficient numerical dissipation to stabilize the strong bow shock and avoid instabilities
  - Without degrading the resolution of the boundary layer to capture accurately the heat flux
- Sensitivity of the numerical method to the quality of the computational grid
  - Multiblock structured grid: adaptation to the flow but costly for complex geometries
  - Unstructured grid: more demanding w.r.t. numerical methods but meshing easier to construct

Quotations from [Candler, JSR 2015]

- *The key concern is adding dissipation to prevent aphysical solutions, without adversely affecting the flow physics.*
- *The standard textbook flux formulation may work beautifully on standard one-dimensional (1-D) test problems, but fail miserably when applied to an actual problem. This is especially true for multidimensional high Mach number flows because it is impossible to design a grid that will be perfectly aligned with strong shock waves without first computing a solution. Thus, it is necessary that the flux functions produce physically meaningful solutions on nonideal grids.*

Left and right-sided fluxes in terms of their average

Expression of the left and the right-sided fluxes

Introducing the arithmetic average of the left and the right-sided fluxes

$$\mathbf{F}_{\mathbf{n}}^{\star}=\frac{1}{2}\left(\mathbf{F}_{\mathbf{n},r}+\mathbf{F}_{\mathbf{n},l}\right)-\frac{1}{2}\left[|\Lambda_l|(\mathbf{U}_l^{\star}-\mathbf{U}_l)+|\Lambda_0|(\mathbf{U}_r^{\star}-\mathbf{U}_l^{\star})+|\Lambda_r|(\mathbf{U}_r-\mathbf{U}_r^{\star})\right].$$

We express them in terms of their average and their difference as

$$\mathbf{F}_{\mathbf{n}}^{-}=\mathbf{F}_{\mathbf{n}}^{\star}-\frac{1}{2}(\lambda_l+\lambda_r)\left(v_{\mathbf{n}}^{\star}-\overline{v}_{\mathbf{n},lr}\right)\begin{pmatrix}0\\ 1\\ \mathbf{0}\\ v_{\mathbf{n}}^{\star}\end{pmatrix},$$

$$\mathbf{F}_{\mathbf{n}}^{+}=\mathbf{F}_{\mathbf{n}}^{\star}+\frac{1}{2}(\lambda_l+\lambda_r)\left(v_{\mathbf{n}}^{\star}-\overline{v}_{\mathbf{n},lr}\right)\begin{pmatrix}0\\ 1\\ \mathbf{0}\\ v_{\mathbf{n}}^{\star}\end{pmatrix}.$$

ARD test case [Annaloro *et al.*, ESA Conf. 2017]

Freestream conditions

Quantities	**ARD**	PRE-X
Mach	**24**	25
Altitude (km)	**65.83**	73.6
Velocity (ms^{-1})	**7212.43**	7205
Density (kgm^{-3})	**1.5869 10^{-4}**	5.546 10^{-5}
Temperature (K)	**224.5**	207
Pressure (Pa)	**10.23**	3.11
Wall temperature (K)	**1500**	1500
Angle of attack (^{o})	**20**	40

Grid: 4.8M tetrahedra (Gmsh)

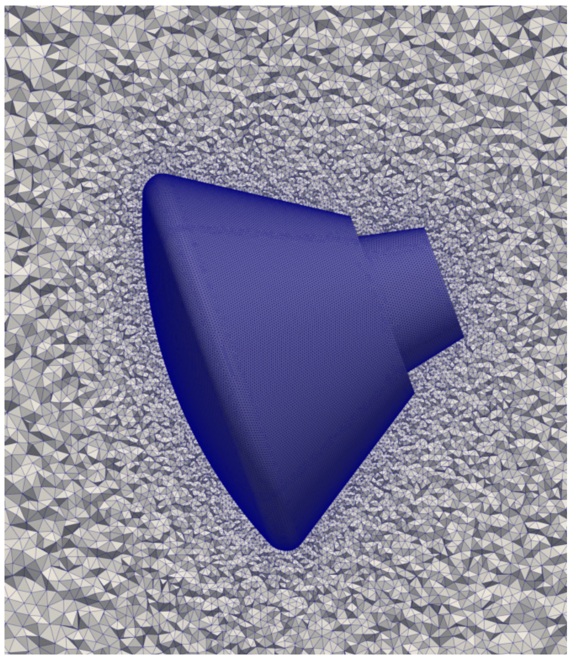

ARD test case [Annaloro *et al.*, ESA Conf. 2017]

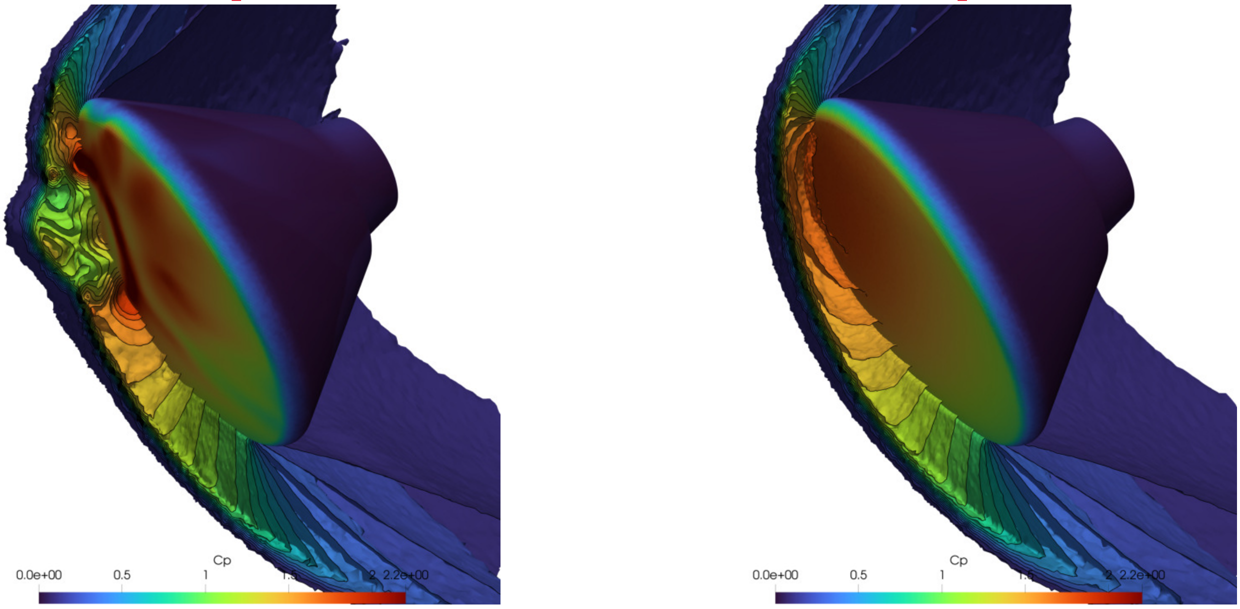

(a) Two-point. (b) Multipoint.

Figure 11: Pressure iso-surfaces.

ARD test case [Annaloro *et al.*, ESA Conf. 2017]

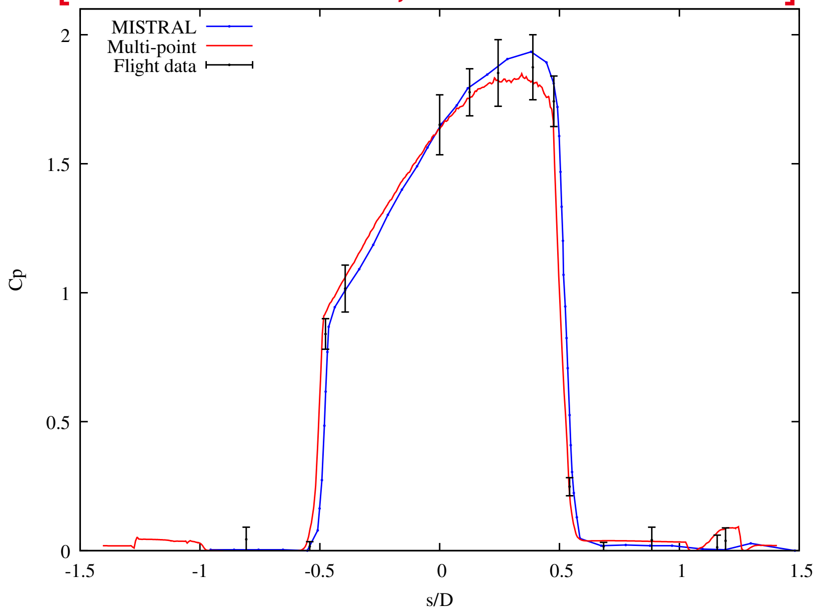

- Pressure coefficient: $C_p = \dfrac{p_{\text{wall}} - p_\infty}{\frac{1}{2}\rho_\infty \mathbf{v}_\infty^2}$ along the trace of $y = 0$
- MISTRAL: Navier-Stokes code from R.Tech